Synthesis and characterisation of Fe(III) and Co(III) complexes of thiazole-containing thiosemicarbazone ligands

Robert J. Laverick[a], Anthony B. Carter[a], Harry A. Klein[a], Anthony J. Fitzpatrick[b], Tony D. Keene[b], Grace G. Morgan[b], Jonathan A. Kitchen[a]*

[a]Chemistry, University of Southampton, Southampton, SO17 1BJ, UK.

[b]School of Chemistry, University College Dublin, Dublin 4, Ireland.

ABSTRACT

Three thiosemicarbazone-based ligands and corresponding Fe(III) and Co(III) coordination complexes have been synthesised and fully characterised. Crystallographic analysis of all ligands and complexes revealed interesting hydrogen bonding and π-stacking packing arrangements. Magnetic susceptibility and EPR measurements indicate that the Fe(III) complexes are in the low spin state from 4 – 300 K. The complexes exhibit significant solution stability (based on UV/vis and NMR data) and the potential for further functionalisation. Such stability gives solution processability and is ideal for the development of advanced supramolecular materials.

1. Introduction

The development of metallosupramolecular assemblies has attracted the interest of scientists for many years and there is now a drive towards developing functional assemblies for supramolecular materials based applications.[1–4] By careful choice of the metal ion a range of applications can be targeted including luminescent systems, catalysts, and magnetically interesting systems. [5–8].[9–11] Thiosemicarbazone-based ligands have been used to generate interesting complexes with a range of potential applications, however one area that appeals to us is their use in Fe(III) spin-crossover (SCO) systems. [12–17] Most examples of thiosemicarbazone-based SCO active complexes use simple thiosemicarbazides and salicylaldehyde (SA) derivatives (*e.g.* **Hthsa**, **Hth5Clsa** and **Hth5Brsa**, Fig. 1). To the best of our knowledge, and despite the large numbers of heterocyclic aldehydes and ketones now available, there have been few studies that have used carbonyl compounds other than SA for investigation into magnetically interesting Fe(III) complexes. Additionally, for SCO-based systems to be useful in areas of nano-technology, solution processability would be advantageous as it allows for simple immobilisation into/onto substrates. Many of the magnetically interesting systems developed to date are significantly labile in solution and undergo ligand displacement giving SCO inactive compounds.[18–22] Therefore developing new ligand systems that can afford favourable coordination environments for SCO and solution stability represents a major challenge in SCO research. Furthermore, ligands that have the ability to be further functionalized (through substituent addition) to allow for targeted immobilization is also desirable, therefore synthetic simplicity and modular synthesis is highly desirable. Thiosemicarbazone-based ligands are ideal for such a purpose as they are readily and reliably constructed from simple precursors allowing introduction of a large range of substituents.[23–32] Here we report the synthesis and characterization of three thiazole containing thiosemicarbazone ligands (**L_1-L_3**, Fig. 1) and their complexation with Fe(III) and Co(III). The magnetic properties of the Fe(III) systems are reported, whilst the low-spin Co(III) systems are reported as a diamagnetic system to the study of solution behavior by NMR techniques. **L_1** has previously been synthesised by Raposo *et al.*[33] and used as part of a study for the recognition of anions. **L_3** has previously been synthesised by Venkatraman *et al.*[34] (as a different polymorph) and used in complexation studies with Ni, Cd, Sn, and Hg.[35–38] However, neither of these studies investigated iron or cobalt complexes for use in supramolecular materials.

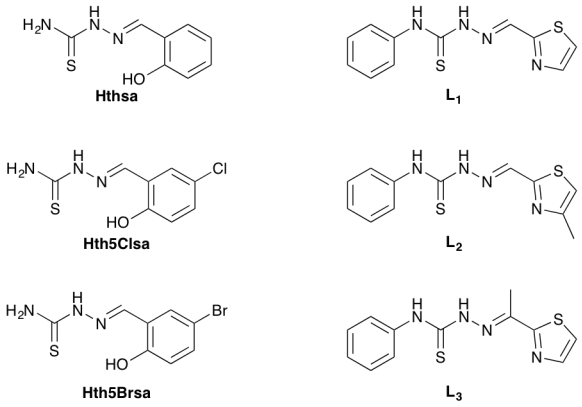

Fig. 1 Thiosemicarbazone ligands known to induce SCO in Fe(III) [**Hthsa**, **Hth5Clsa**, **Hth5Brsa**] (left) and ligands used in this study (right).

2. Experimental

2.1 General

All reagents were purchased from commercial sources and used without further purification. ^{1}H, and ^{13}C{^{1}H} NMR spectra were recorded on a Bruker DPX400 NMR spectrometer at 300 K. Chemical shifts are reported in parts per million and referenced to the residual solvent peak (*d_6-DMSO*: ^{1}H δ 2.50 ppm, ^{13}C δ 39.52 ppm). Coupling constants (J) are reported in Hertz (Hz). Standard

conventions indicating multiplicity were used: m = multiplet, t = triplet, d = doublet, s = singlet, dd[appt] = doublet of doublets which appears as a triplet. Infrared spectra were recorded using a ThermoScientific Nicolet iS10 FTIR spectrometer between 600 and 4000 cm^{-1}. Mass spectrometry samples were analysed using a MaXis (Bruker Daltonics, Bremen, Germany) mass spectrometer equipped with a Time of Flight (TOF) analyser. Samples were introduced to the mass spectrometer via a Dionex Ultimate 3000 autosampler and uHPLC pump [Gradient 20% acetonitrile (0.2% formic acid) to 100% acetonitrile (0.2% formic acid) in five minutes at 0.6 mL min^{-1}. Column: Acquity UPLC BEH C18 (Waters) 1.7 micron 50 x 2.1mm]. High-resolution mass spectra were recorded using positive/negative ion electrospray ionisation. Single-crystal X-ray diffraction data was collected at 100 K on a Rigaku AFC12 goniometer equipped with an enhanced sensitivity (HG) Saturn 724+ detector mounted at the window of an FR-E+ Superbright Mo-K_α rotating anode generator (λ = 0.71075 Å) with HF or VHF varimax optics.[39] Unit cell parameters were refined against all data and an empirical absorption correction applied in either CrystalClear[40] or CrysalisPro.[41] All structures were solved by direct methods using SHELXS-2013[42] and refined on F_0^2 by SHELXL-2013[42] using Olex2.[43] The crystallographic data are summarised below. CCDC entries 1498845 - 1498852 contain the crystallographic data for the structures reported in this article.

UV-Vis absorption spectra were recorded on a PerkinElmer Lambda 265 Spectrophotometer between 200 and 900 nm. Variable temperature magnetic susceptibility for crystalline samples of all three Fe(III) complexes were recorded on a Quantum Design MPMS® XL-7 SQUID magnetometer at 0.1 T. Magnetic susceptibility was recorded in the range of 400 to 10 K at 3 K/min temperature scan rate. EPR data was collected between 283 and 373 K on a polycrystalline sample using a Magnettech mS200 X-band EPR working at 9.381 GHz with magnetic field centred at 300 mT and a field sweep of 400 mT. Modulation amplitude of 0.5 mT was used in conjunction with a microwave power of 0.1 mW and a gain of 10.

2.2 Ligand Synthesis

2.2.1 Synthesis of ***L₁:*** To a stirred solution of 4-phenylthiosemicarbazide (200 mg, 1.20 mmol) in methanol (30 mL), 2-thiazolecarboxaldehyde (105 µL, 1.20 mmol) was added. The light yellow solution was left to stir for 24 hours. The resulting dark yellow solution was concentrated *in vacuo* resulting in the precipitation of a yellow solid. This was filtered and then washed with diethyl ether (2 x 25 mL), the resulting yellow solid was crystallized from methanol (20 mL) resulting in a light yellow crystalline solid suitable for single crystal X-ray diffraction. Yield: 181 mg (69%); HRMS ESI+ m/z: 285.0234 [**L₁** + Na]$^+$, $C_{11}H_{10}N_4S_2Na$ requires: 285.0239; IR: ν = 3322, 3297, 3054, 1634, 1598, 1279, 1176, 1166, 1013 cm^{-1}; λ_{max} (MeOH) =343 nm, ε = 21,500 $Lmol^{-1}cm^{-1}$; ^{1}H NMR (400 MHz, DMSO-d_6): δ 12.09 (s, 1H, N*H*), 10.10 (s, 1H, N*H*), 8.39 (s, 1H, Im*H*), 7.96 (d, *J* = 3.2 Hz, 1H, Thia*H*), 7.86 (d, *J* = 3.2 Hz, 1H, Thia*H*), 7.56 – 7.53 (m, 2H, Ph*H*), 7.41-7.35 (m, 2H, Ph*H*), 7.23 (m, 1H, Ph*H*). ^{13}C NMR (101 MHz, DMSO-d_6): 122.29, 125.59, 125.86, 128.16, 137.29, 138.88, 144.00, 163.56, 176.28. Yellow rod-like crystals (0.35 × 0.08 × 0.07 mm) of **L₁** were obtained from hot recrystallisation from methanol. **Crystal Data** for $C_{11}H_{10}N_4S_2$ (*M* =262.35 g/mol): monoclinic, space group $P2_1/c$ (no. 14), *a* = 13.5767(10) Å, *b* = 5.3420(4) Å, *c* = 17.5065(11) Å, β = 110.324(6)°, *V* = 1190.64(15) Å^3, *Z* = 4, *T* = 100(2) K, μ(MoK_α) = 0.428 mm^{-1}, *Dcalc* = 1.464 g/cm^3, 8078 reflections measured (4.962° ≤ 2Θ ≤ 55.082°), 2728 unique (R_{int} = 0.0273, R_{sigma} = 0.0221) which were used in all calculations. The final R_1 was 0.0276 (I > 2σ(I)) and wR_2 was 0.0715 (all data).

2.2.2 Synthesis of ***L₂:*** To a stirred solution of 4-phenylthiosemicarbazide (200 mg, 1.20 mmol) in methanol (30 mL), 4-methyl-2-thiazolecarboxaldehyde (129 µL, 1.20 mmol) was added. The solution was stirred for 24 hours. The resulting dark yellow solution was concentrated *in vacuo*, leaving a dark yellow oil. This was triturated in diethyl either (20 mL) and decanted before being recrystallized from methanol (20 mL) resulting in a dark yellow crystalline solid. Yield: 133 mg (48%); HRMS ESI+ m/z: 299.0395 [**L₂** + Na]$^+$, $C_{12}H_{12}N_4S_2Na$ requires: 299.0396; IR: ν = 3317, 3107, 3054, 1596, 1538, 1236, 1176, 1165, 1031 cm^{-1}; λ_{max} (MeOH) =349 nm, ε = 22,600 $Lmol^{-1}cm^{-1}$; ^{1}H NMR (300 MHz, DMSO-d_6) δ 12.05 (s, 1H, N*H*), 10.04 (s, 1H, N*H*), 8.33 (s, 1H, Im*H*), 7.54 (m, 2H, Ph*H*), 7.40 – 7.34 (m, 3H, Ph*H* & Thia*H*), 7.24-7.19 (m, 1H, Ph*H*), 2.39 (s, 3H, Methyl*H*). ^{13}C NMR (101 MHz, DMSO-d_6): 17.17, 117.17, 126.00. 126.29, 128.61, 137.83, 139.36, 153.85, 163.07, 176.66. Orange rod-like crystals (0.27 × 0.05 × 0.04 mm) of **L₂** were obtained from hot recrystallisation from methanol. **Crystal Data** for $C_{12}H_{12}N_4S_2$ (*M* =276.38 g/mol): orthorhombic, space group $P2_12_12_1$ (no. 19), *a* = 5.004(5) Å, *b* = 15.83(2) Å, *c* = 16.73(2) Å, *V* = 1325(3) Å^3, *Z* = 4, *T* = 373.3 K, μ(MoK_α) = 0.389 mm^{-1}, *Dcalc* = 1.385 g/cm^3, 4836 reflections measured (5.694° ≤ 2Θ ≤ 50.988°), 2427 unique (R_{int} = 0.0305, R_{sigma} = 0.0489) which were used in all calculations. The final R_1 was 0.0440 (I > 2σ(I)) and wR_2 was 0.0767 (all data).

2.2.3 Synthesis of ***L₃***: To a stirred solution of 4-phenylthiosemicarbazide (100 mg, 0.6 mmol) in ethanol (10 mL), 2-acetylthiazole (70 µL, 0.6 mmol) was added. The solution was refluxed for 3 hours. The solution was concentrated resulting in the precipitation of a yellow crystalline solid that was filtered, washed with diethyl ether (2 x 25 mL) and dried *in vacuo*. Yield 84 mg, 51%. HRMS ESI+ m/z: 277.0574 [**L₃** + H]$^+$, $C_{12}H_{13}N_4S_2$ requires: 277.0576; IR ν = 3238, 3112, 3037, 1651, 1479, 1371, 1046 cm^{-1} ; λ_{max} (MeOH) =339 nm, ε = 20,500 $Lmol^{-1}cm^{-1}$; ^{1}H NMR (400 MHz, DMSO-d_6) δ 11.01 (s, 1H, N*H*), 9.92 (s, 1H, N*H*), 7.91 (d, *J* = 3.2 Hz, 1H, Thia*H*), 7.82 (d, *J* = 3.2 Hz, 1H, Thia*H*), 7.63 – 7.59 (m, 2H, Ph*H*), 7.38 (dd[appt], *J* = 8.1 Hz, 2H, Ph*H*), 7.23 – 7.19 (m, 1H, Ph*H*), MethylH signal masked by solvent peaks. ^{13}C NMR (101 MHz, DMSO-d_6) δ 14.44, 123.22, 125.53, 125.89, 128.72, 139.36, 143.82, 145.57, 167.25, 177.30. Yellow plate like crystals (0.4 × 0.2 × 0.09 mm) of **L₃** were grown from the slow evaporation of methanol. **Crystal Data** for $C_{12}H_{12}N_4S_2$ (*M* =276.37 g/mol): triclinic, space group *P*-1 (no. 2), *a* = 8.211 Å, *b* = 8.581 Å, *c* = 9.241 Å, α = 85.44°, β = 79.51°, γ = 80.63°, *V* = 630.8 Å^3, *Z* = 2, *T* = 100 K, μ(MoK_α) = 0.408 mm^{-1}, *Dcalc* = 1.455 g/cm^3, 5325 reflections measured (6.192° ≤ 2Θ ≤ 50.99°), 2326 unique (R_{int} = 0.0144, R_{sigma} = 0.0155) which were used in all calculations. The final R_1 was 0.0296 (I > 2σ(I)) and wR_2 was 0.0812 (all data).

2.3 Complex synthesis

Unless stated otherwise, to a stirred solution of metal salt $Fe(NO_3)_3{\cdot}9H_2O$ (24.0 mg, 0.06 mmol) or $Co(BF_4)_2{\cdot}6H_2O$ (20.2 mg, 0.06 mmol)) in methanol (20 mL), ligand (**L₁**, **L₂** or **L₃**) (0.12 mmol) was added. The resulting solution was stirred vigorously

for an hour at room temperature, before being subjected to vapour diffusion of diethyl either, which resulted in very dark crystals:

2.3.1 [Fe(L1)2](NO3) - Yield: 30.4 mg (80%); HRMS ESI+ m/z: 577.9890 [Fe(**L1**)2 – NO3]+, $C_{22}H_{18}N_8S_4Fe$ requires: 577.9881. IR: ν= 3179, 3126, 3028, 3008, 1594, 1542, 1309, 1283, 1193, 1181 (NN), 1001 cm^{-1}. UV/vis (MeOH) λ_{max} = 402 nm, ε = 43,650 L mol^{-1} cm^{-1}. Dark orange, plate like crystals of [Fe(**L1**)2](NO3)·H2O (0.48 × 0.09 × 0.04 mm) were grown by diffusion of diethyl ether into the reaction solution. **Crystal Data** for $C_{22}H_{20}FeN_9O_4S_4$ (*M* =658.56 g/mol): monoclinic, space group $P2_1/n$ (no. 14), *a* = 12.0840(8) Å, *b* = 14.3302(10) Å, *c* = 15.8785(11) Å, *β* = 105.4500(10)°, *V* = 2650.3(3) Å3, *Z* = 4, *T* = 100.15 K, μ(MoKα) = 0.934 mm^{-1}, *Dcalc* = 1.651 g/cm3, 15780 reflections measured (6.036° ≤ 2Θ ≤ 50.998°), 4914 unique (R_{int} = 0.0303, R_{sigma} = 0.0266) which were used in all calculations. The final R_1 was 0.0347 (I > 2σ(I)) and wR_2 was 0.0950 (all data).

2.3.2 [Fe(L2)2](NO3) - Yield: 30.1 mg (76%); HRMS ESI+ m/z: 606.0204 [Fe(**L2**)2 – NO3]+, $C_{24}H_{22}N_8S_4Fe$ requires: 606.0194. IR: ν= 3026, 2953, 2920, 1604, 1592, 1335, 1291, 1207, 1182, 982.cm^{-1}. UV/vis (MeOH) λ_{max} = 406 nm, ε = 43,240 L mol^{-1} cm^{-1}. Dark orange, plate like crystals of [Fe(**L2**)2](NO3)·H2O (0.31 × 0.10 × 0.09 mm) were grown by diffusion of diethyl ether into the reaction solution. **Crystal Data** for $C_{24}H_{24}FeN_9O_4S_4$ (*M* =686.61 g/mol): monoclinic, space group $P2_1/c$ (no. 14), *a* = 9.0741(5) Å, *b* = 14.1019(10) Å, *c* = 22.4772(16) Å, *β* = 98.271(2)°, *V* = 2846.3(3) Å3, *Z* = 4, *T* = 100.15 K, μ(MoKα) = 0.873 mm^{-1}, *Dcalc* = 1.602 g/cm3, 16157 reflections measured (5.406° ≤ 2Θ ≤ 50.998°), 5261 unique (R_{int} = 0.0724, R_{sigma} = 0.0750) which were used in all calculations. The final R_1 was 0.0528 (I > 2σ(I)) and wR_2 was 0.1317 (all data).

2.3.3 [Fe(L3)2](NO3) - Yield: 30.1 mg (76%); HRMS ESI+ m/z: 606.0189 [Fe(**L3**)2 – NO3]+, $C_{24}H_{22}N_8S_4Fe$ requires: 606.0194. IR: ν= 3223, 3076, 1596, 1364, 1296, 1244, 1038, 690 cm^{-1} UV/vis (MeOH) λ_{max} = 397 nm, ε = 43,120 L mol^{-1} cm^{-1}. Dark orange, plate like crystals of [Fe(**L3**)2](NO3)· ¾H2O (0.19 × 0.12 × 0.05 mm) were grown by diffusion of diethyl ether into the reaction solution. **Crystal Data** for $C_{24}H_{23.5}FeN_9O_{3.75}S_4$ (*M* =682.11 g/mol): orthorhombic, space group $Pna2_1$ (no. 33), *a* = 14.0509(8) Å, *b* = 22.7382(13) Å, *c* = 8.6415(5) Å, *V* = 2760.9(3) Å3, *Z* = 4, *T* = 100.15 K, μ(MoKα) = 0.899 mm^{-1}, *Dcalc* = 1.641 g/cm3, 11487 reflections measured (4.714° ≤ 2Θ ≤ 49.99°), 4787 unique (R_{int} = 0.0483, R_{sigma} = 0.0829) which were used in all calculations. The final R_1 was 0.0687 (I > 2σ(I)) and wR_2 was 0.1807 (all data), twinned data refinement scales for twin law –h, k, -l: 0.67(5) 0.33(5).

2.3.4 [Co(L1)2](BF4) - Yield: 27.0 mg (68%); MS ESI+ m/z: 580.9855 [Co(L1)2 – BF4]+, $C_{22}H_{18}CoN_8S_4$ requires: 580.9864; IR: ν= 3328, 3137, 3078, 3038, 2973, 1593, 1526, 1417, 1398 1314, 1293, 1191, 1149, 1000 cm^{-1}; ^{1}H NMR (400 MHz, DMSO-d_6): δ 10.60 (s, 2H, N*H*), 9.02 (s, 2H, Im*H*), 8.06 (d, *J* = 3.4 Hz, 2H, Thia*H*), 7.68 (d, *J* = 3.4 Hz, 2H, Thia*H*), 7.60 (d, *J* = 8.0 Hz, 4H, Ph*H*), 7.39 – 7.34 (m, 4H, Ph*H*), 7.12 (m, 2H, Ph*H*). Small, dark red, plate like crystals of [Co(L1)2](BF4)·½H2O (0.09 × 0.04 × 0.01 mm) were grown by diffusion of diethyl ether into the reaction solution. Crystal Data for $C_{22}H_{19}BN_8O_{0.5}F_4S_4Co$ (*M* =677.43 g/mol): monoclinic, space group $P2_1/n$ (no. 14), *a* = 12.120(2) Å, *b* = 14.421(3) Å, *c* = 15.666(3) Å, *β* = 103.54(3)°, *V* = 2662.1(10) Å3, *Z* = 4, *T* = 100.15 K, μ(MoKα) = 1.020 mm^{-1}, *Dcalc* = 1.690 g/cm3, 15530 reflections measured (4.464° ≤ 2Θ ≤ 50.996°), 4948 unique (R_{int} = 0.0427, R_{sigma} = 0.0420) which were used in all calculations. The final R_1 was 0.0398 (I > 2σ(I)) and wR_2 was 0.1000 (all data).

2.3.5 [Co(L2)2](BF4) - Yield: 29.3 mg (71%); MS ESI+ m/z: 609.0188 [Co(**L1**)2 – BF4]+, $C_{24}H_{22}CoN_8S_4$ requires: 609.0177; IR: ν= 3308, 3105, 3076, 3038, (NN), 987; λ_{max} =402 nm; ^{1}H NMR (400 MHz, DMSO-d_6): δ 10.65 (s, 2H, N*H*), 9.01 (s, 2H, Im*H*), 7.72 (s, 2H, Thia*H*), 7.58 (d, *J* = 8.0 Hz, 4H, Ph*H*), 7.37 (dd[appt], *J* = 7.7 Hz, 4H, Ph*H*), 7.12 (t, *J* = 7.4 Hz, 2H, Ph*H*), 2.22 (s, 6H, Methyl*H*). Small, dark red, needle like crystals of [Co(**L2**)2](BF4)·Et2O (0.12 × 0.06 × 0.02 mm) were grown by diffusion of diethyl ether into the reaction solution. **Crystal Data** for $C_{26}H_{27}BCoF_4N_8O_{0.5}S_4$ (*M* =733.53 g/mol): monoclinic, space group $P2_1/c$ (no. 14), *a* = 10.9533(8) Å, *b* = 12.7844(9) Å, *c* = 23.1491(16) Å, *β* = 93.5960(10)°, *V* = 3235.2(4) Å3, *Z* = 4, *T* = 100.15 K, μ(MoKα) = 0.846 mm^{-1}, *Dcalc* = 1.506 g/cm3, 30141 reflections measured (5.288° ≤ 2Θ ≤ 50°), 5678 unique (R_{int} = 0.0575, R_{sigma} = 0.0312) which were used in all calculations. The final R_1 was 0.0511 (I > 2σ(I)) and wR_2 was 0.1381 (all data).

2.3.6 [Co(L3)2](BF4) - To a stirred solution of metal salt Co(BF4)2·6H2O (12.7 mg, 0.04 mmol)) in methanol (20 mL), ligand (L3) (0.07 mmol) was added. Yield: 17.8 mg (70%); MS ESI+ m/z: 609.0181 [Co(L1)2 – BF4]+, $C_{24}H_{22}CoN_8S_4$ requires 609.0177; IR: ν= 3228, 2161, 1496, 1431, 1047, 750, 575 cm^{-1}; λ_{max} =402 nm; ^{1}H NMR (400 MHz, DMSO-d_6): δ 10.74 – 9.90 (bs, 2H, N*H*), 8.08 (d, *J* = 3.5 Hz, 2H, Thia*H*), 7.69 – 7.66 (m, 6H, Ph*H* & Thia*H*), 7.37 (dd[appt], *J* = 7.8 Hz, 4H, Ph*H*), 7.09 (t, *J* = 7.4 Hz, 2H, Ph*H*), 2.95 (s,

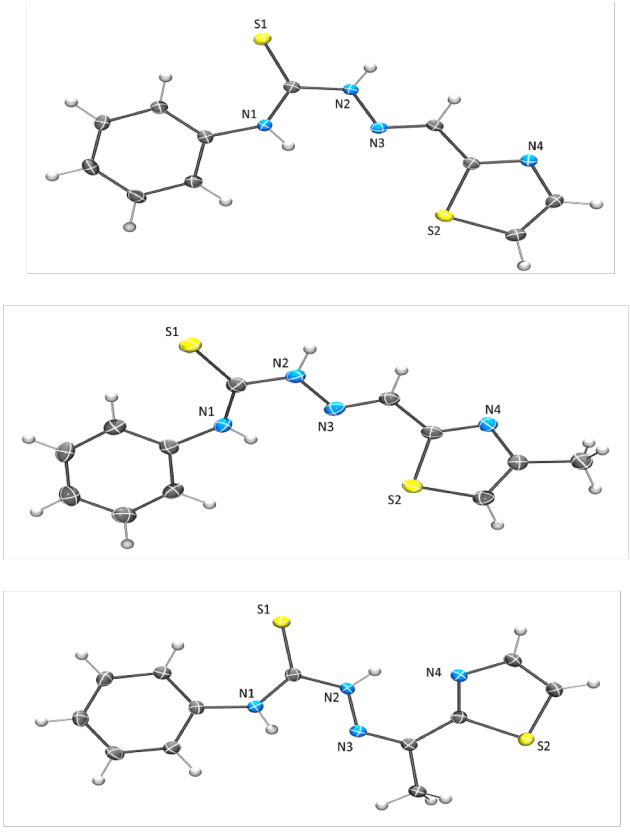

Fig. 2 Molecular structures of **L1** (top), **L2** (middle) and **L3** (bottom). Thermal ellipsoids shown at 50% probability.

6H, Methyl*H*). Despite repeated attempts, and under a variety of conditions only very poor quality dark orange block like crystals (0.11 × 0.10 × 0.08 mm) were grown by diffusion of diethyl ether into a methanol solution. The data quality was sufficiently poor that no packing interactions are discussed and the molecular structure serves to show the connectivity of the [Co(**L3**)$_2$] cation only. **Crystal Data** for $C_{24}H_{21}CoN_8S_4$ (M =608.66 g/mol): orthorhombic, space group *Pbca* (no. 61), a = 8.4306(2) Å, b = 21.5049(6) Å, c = 33.7844(11) Å, V = 6125.1(3) Å^3, Z = 8, T = 100 K, μ(MoKα) = 0.860 mm^{-1}, *Dcalc* = 1.320 g/cm^3, 48295 reflections measured (3.788° ≤ 2Θ ≤ 49.998°), 5383 unique (R_{int} = 0.0609, R_{sigma} = 0.0380) which were used in all calculations. The final R_1 was 0.0750 (I > 2σ(I)) and wR_2 was 0.2076 (all data). The structure was treated with a smtbx solvent mask in Olex2 to remove the severely disordered BF_4^- counter anion and an interstitial water molecule.

3. Results and Discussion

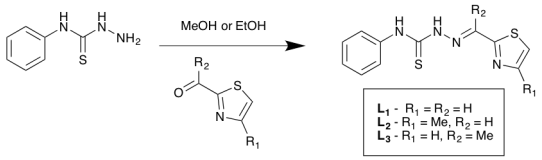

Scheme 1 General synthesis of **L$_1$** – **L$_3$**

with respect to the angles formed between the thiazole - thiosemicarbazone mean-plane (4.7°) and the thiosemicarbazone - phenyl mean-plane (14.3°). The thiourea moiety adopts an *anti*-conformation and the imine bond adopts a *trans* configuration (*i.e.* thiazole group and thiourea NH are *trans*). When examining the long range packing two perpendicular planes of ligand run though the crystal along the b axis (Fig. S44, ESI), this is facilitated through intermolecular hydrogen bonding [N(3)···N(1)' = 2.980(2) Å and <(N(3)-H(3X)···N(1)')= 164°]. Small, dark orange, rod-like crystals of **L$_2$** were obtained from hot recrystallisation from methanol and crystallised in the chiral orthorhombic space group $P2_12_12_1$, and contained one molecule in the asymmetric unit. The ligand conformation is very similar to that of **L$_1$**, where it adopts a relatively flat structure with respect to the angles formed between the thiazole - thiosemicarbazone mean-plane (11.4°) and the thiosemicarbazone - phenyl mean-plane (5.8°). Again the thiourea moiety adopts an *anti*-conformation and the imine bond adopts a *trans* configuration as per **L$_1$**. The long range packing differs significantly to **L$_1$** as the intermolecular hydrogen bonding

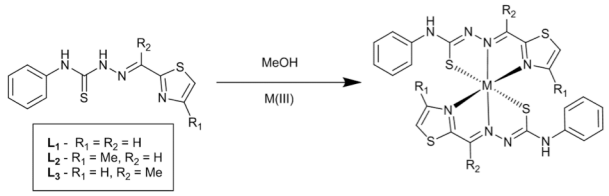

Scheme 2 Complexation of ligands **L$_1$** – **L$_3$** with Fe(III) or Co(III).

3.1 Ligand synthesis and characterisation

Ligands **L$_1$** - **L$_3$** (Fig. 2) were synthesised by the same general procedure (Scheme 1) using a stoichiometric reaction between the thiazole carbonyl (2-thiazolecarboxaldehyde, 4-methyl-2-thiazolecarboxaldehyde or 2-acetylthiazole) and 4-phenylthiosemicarbazide in refluxing methanol or ethanol to yield **L1**, **L2** and **L3** respectively. Following the reaction, concentration of solvent resulted in pale orange/yellow solids in moderate yields (48 – 69%). **L$_1$** – **L$_3$** were fully characterised using ^{1}H-NMR, ^{13}C-NMR, IR, UV/vis, mass spectrometry and X-ray crystallography. All spectroscopic data was consistent with the formation of the desired thiosemicarbazone ligands (see supporting information). **L$_1$** and **L$_3$** match the literature data.[30,31] Large pale yellow crystals of **L$_1$** were obtained by hot recrystallisation from methanol. The ligand crystallised in the monoclinic space group $P2_1/c$, with one molecule in the asymmetric unit. The ligand adopts a relatively planar structure in **L$_2$** [N(3)···N(1)' = 3.025(5) Å and <(N(3)-H(3X)···N(1)')= 158°] results in a helical hydrogen bonded 1D chain along the crystallographic a-axis. Small pale yellow crystals of **L$_3$** were grown from the slow evaporation of methanol. **L$_3$** crystallised in the triclinic space group *P*-1 and contained one molecule in the asymmetric unit. Like **L$_1$** and **L$_2$** the structure of **L$_3$** is again planar with small mean-plane angles (<11°) between the three main functional groups. The thiourea moiety adopts the *anti*-conformation as per the previous systems. However, unlike **L$_1$** and **L$_2$** the imine in **L$_3$** adopts a *cis*-configuration orientating the thiazole nitrogen into a position to be involved in a second intramolecular hydrogen bonding interaction between the second thiourea NH group and the thiazole nitrogen atom [N(3)···N(1) = 2.698(2) Å and <(N(3)-H(3X)···N(1))= 136.2(2)°]. With both NH donors involved in intramolecular hydrogen bonding, extension of the structure via H-bonding does not occur, instead there are weak off-set face to face π···π stacking interactions between the

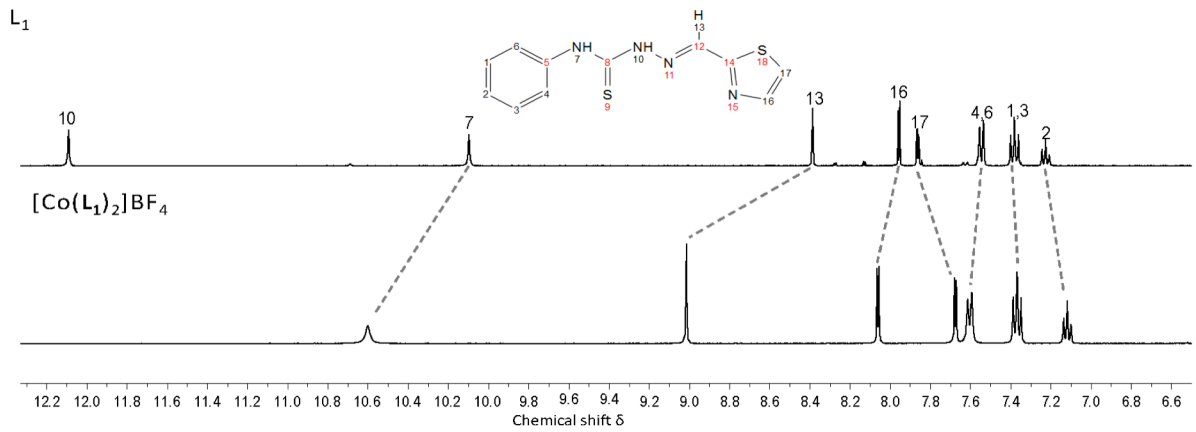

Fig. 3 Stacked plot of ^{1}H-NMR spectra of **L$_1$** (top) and [Co(**L$_1$**)$_2$](BF$_4$) (bottom) recorded in DMSO-d$_6$ highlighting shifted proton signals on complexation

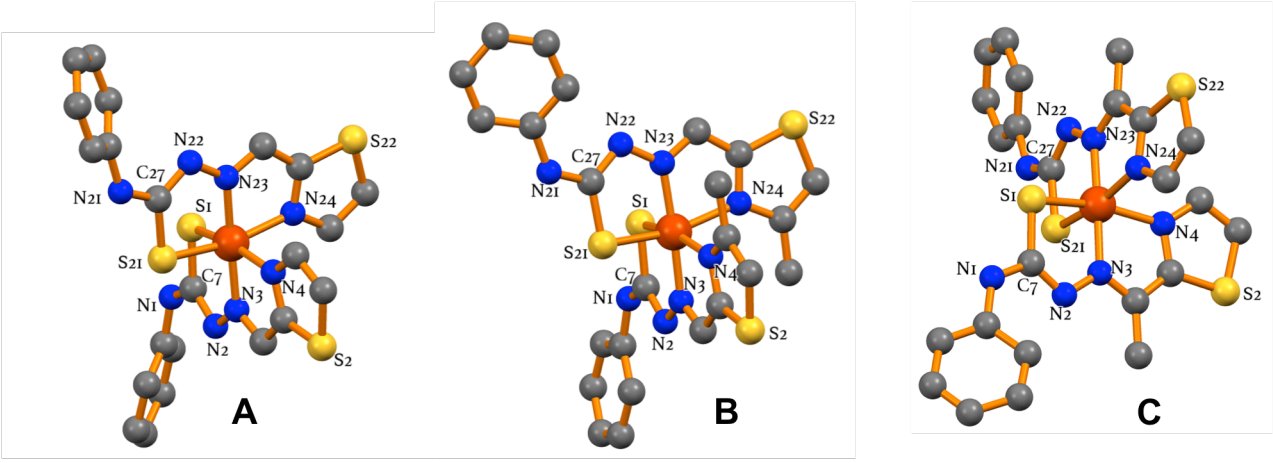

	L_1	$[Fe(L_1)_2]NO_3.H_2O$	$[Co(L_1)_2]BF_4.H_2O$	L_2	$[Fe(L_2)_2]NO_3.H_2O$	$[Co(L_2)_2]BF_4.Et_2O$	L_3	$[Fe(L_3)_2]NO_3.¾H_2O$
N2 - C7 / Å	1.361(2)	1.333(3)	1.334(4)	1.367(5)	1.324(5)	1.321(4)	1.368(2)	1.294(16)
S1 - C7 / Å	1.673(1)	1.742(3)	1.732(3)	1.665(4)	1.764(4)	1.752(3)	1.677(2)	1.748(12)
N22 - C27 / Å	-	1.327(3)	1.322(4)	-	1.330(4)	1.336(4)	-	1.290(14)
S21 - C27 / Å	-	1.760(2)	1.744(3)	-	1.751(4)	1.739(3)	-	1.750(12)
M1 - S1 / Å	-	2.220(7)	2.228(1)	-	2.220(11)	2.2108(9)	-	2.222(3)
M1 - S21 / Å	-	2.226(7)	2.225(1)	-	2.226(10)	2.2218(9)	-	2.207(3)
M1 - N4 / Å	-	1.975(2)	1.945(2)	-	2.019(3)	1.978(3)	-	1.984(10)
M1 - N3 / Å	-	1.931(2)	1.907(3)	-	1.928(3)	1.890(3)	-	1.925(9)
M1 - N24 / Å	-	1.987(2)	1.964(3)	-	2.034(3)	1.994(3)	-	1.966(9)
M1 - N23 / Å	-	1.930(2)	1.902(3)	-	1.924(3)	1.890(3)	-	1.916(9)
Σ / ⁰	-	68.7(8)	53.6(11)	-	71.2(12)	49.7(12)	-	71.6(6)
Cis angle range / ⁰	-	80.6 - 99.8 (1)	81.9 - 99.2 (1)	-	81.1 - 101.6 (1)	83.1 - 100.6 (1)	-	80.7 - 104.2 (13)

Fig. 4 Molecular structures (top) of $[Fe(L_1)_2](NO_3)\cdot H_2O$ (A), $[Fe(L_2)_2](NO_3)\cdot H_2O$ (B), and $[Fe(L_3)_2](NO_3)\cdot ¾H_2O$ (C) showing numbering scheme. Nitrate counter anion, interstitial water molecules and hydrogen atoms are omitted for clarity – see ESI for additional figures of the molecular structures. Table of selected bond lengths and angles (bottom) for all structurally characterised ligands and complexes. Σ values for complexes are also tabulated for structurally characterised Fe(III) and Co(III) complexes.

thiazole and the phenyl rings on neighbouring molecules [centroid⋯centroid = 3.74 Å, Fig. S45, ESI].

3.2 Complex synthesis

Complexation reactions (Scheme) were carried out in methanol between **L1**-**L3** and $Fe(NO_3)_3\cdot 9H_2O$ and $Co(BF_4)_2\cdot 6H_2O$ using a 2:1 L:M ratio. In each case the addition of a methanolic solution of metal salt to the methanolic ligand solution resulted in a dramatic colour change from pale yellow to very dark orange/brown. The dark solutions were stirred vigorously whilst open to the air at room temperature for 1 h before being subjected to vapour diffusion of diethyl ether. In all cases this gave very dark red to orange crystals in reasonable yields (68-80%). The complexes all adopt the general formula [M(**L**)2](anion)·solvent with the metal in the +3 oxidation state. The ligand binds through the thioenolate form rather than the thioketo form giving a mono-negative charge on the ligand.

3.3 Infrared, Mass Spectrometry, NMR and UV/vis spectroscopy

Infrared spectroscopy provides a valuable tool for analysing these thiosemicarbazone systems. On binding, the ligand undergoes a tautomerism resulting in small spectral changes (C=S to C-S). The comparison between ligands and complexes is shown in Fig S13 – S15, ESI. The IR spectra of the complexes also show the expected signals for the NO_3^- and BF_4^- anions in the Fe(III) and Co(III) complexes respectively. High-resolution mass spectra of all ligands and complexes were collected and showed the expected peaks and isotopic distributions for all ligands and complexes (Fig. S19 – S27, ESI). Electronic spectra of ligands and iron complexes were obtained in MeOH and in the solid state (Fig S16 – S18, ESI). Spectra of **L1**-**L3** (*ca.* $1x10^{-5}$ mol L^{-1} in MeOH) displayed similar spectral features with intense absorptions at λ_{max} ~ 350 nm (ε 20,500 – 22,500 $Lmol^{-1}cm^{-1}$). Absorption spectra of Fe(III) complexes (*ca.* $1x10^{-5}$ mol L^{-1} in MeOH) showed intense broad charge-transfer absorptions at ~ 400 nm (ε ~43,000 $Lmol^{-1}cm^{-1}$) accounting for the intense colour of the Fe(III) complexes. The Fe(III) complexes appeared to be stable in solution over long periods of time as the spectra collected some 4 weeks later were unchanged. ^{1}H-NMR spectra were collected of the three Co(III) complexes in d_6-DMSO (Fig. S2, S5, S8, ESI). In each case there was a significantly shifted spectrum when compared to the respective ligand spectrum (*e.g.* the imine protons display a ~0.6 ppm downfield shift) and loss of one NH resonance indicating successful complexation (Fig. 3, S3, S6, S9, ESI). Again the complexes exhibited significant solution stability, as spectra collected 4 weeks apart were unchanged. The observed solution stability indicates that these thiosemicarbazone complexes are potentially ideal for development of supramolecular materials and thus should be suitable for a variety of immobilisation techniques where solution processability is required (*e.g.* gels, Langmuir-Blodgett films and incorporation into polymers).

3.4 Crystallographic analysis of Fe^{3+} complexes

Crystals of $[Fe(L_1)_2](NO_3)\cdot H_2O$, $[Fe(L_2)_2](NO_3)\cdot H_2O$, and $[Fe(L_3)_2](NO_3)\cdot ¾H_2O$ were obtained as large red/orange rods or plates by diffusion of diethyl ether into methanolic solutions of the complexes and the low temperature (100 K) structures obtained (Fig. 4). $[Fe(L_1)_2](NO_3)\cdot H_2O$ crystallised in the monoclinic spacegroup $P2_1/c$, $[Fe(L_2)_2](NO_3)\cdot H_2O$ crystallised in the monoclinic space group $P2_1/n$ and $[Fe(L_3)_2](NO_3)\cdot ¾H_2O$ crystallised in the orthorhombic space group $Pna2_1$. In all cases the asymmetric unit contained one complete molecule and one

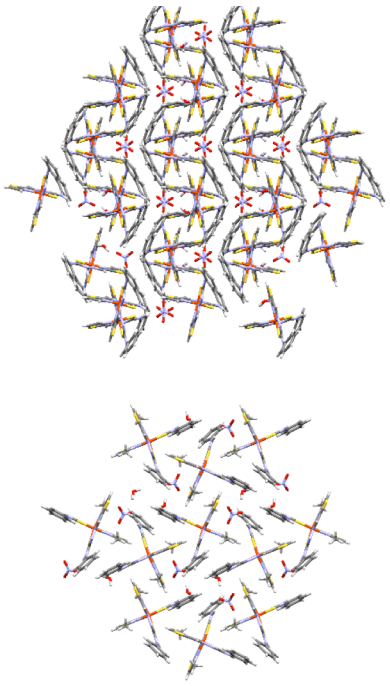

Fig. 5 Packing diagrams of $[Fe(\mathbf{L_1})_2](NO_3)\cdot H_2O$ (top) showing spiralled layer formation and $[Fe(\mathbf{L_2})_2](NO_3)\cdot H_2O$ showing both the orientation of the packing along the crystallographic c-axis (bottom).

interstitial water molecule (either full or ¾ occupancy). The general structure of each complex is similar where the Fe(III) centre adopts a distorted octahedral geometry with an S_2N_4 coordination sphere. Bond lengths and angles are consistent with low-spin Fe(III) and are summarised in Figure 4. Analysis of the distortion parameter, Σ (sum of the deviation of the *cis* bond angles from 90°),[18,21,44,45] indicated relatively small distortion from purely octahedral geometry (ranging from 68.7° to 71.5°). The data also reaffirms the IR spectroscopic interpretation of changes in bond lengths for the C=S and C-N bonds (Fig. 4). Packing in the solid state is an important area of consideration for potential SCO systems as intermolecular interactions can increase communication between neighbouring molecules and therefore enhance the cooperative nature of the magnetism. In these systems the ligands have many functional groups capable of extending the structure through supramolecular interactions (*e.g.* H-bonding, π···π stacking, anion···π and CH···π interactions) making analysis of the packing important. $[Fe(\mathbf{L_1})_2](NO_3)\cdot H_2O$ displays hydrogen bonding interactions between thioamide NH groups on neighbouring complexes (N(4)' and N(24)) and a nitrate counter anion [N(4)'···O(102) = 2.877(3) Å and <(N(4)'-H(4X)'···O(102))= 172°; N(24)···O(102) = 2.845(3) Å and <(N(24)-H(24X)···O(102))= 160°] where the NO_3^- acts as a bridge between two complex molecules (Fig S44, ESI). The interstitial water molecule further bridges the nitrate anion to a third molecule by acting as a hydrogen bond donor to a nitrate oxygen atom (O(100)) and the thioenolate nitrogen atom (N(23)') on a neighbouring molecule [O(200)···O(100) = 2.856(3) Å and <(O(200)-H(20Y) ···O(100))= 176°; O(200)···N(23)" = 2.924(3) Å and <(O(200)-H(20Y)···N(23)")= 174°]. The NH and OH hydrogen bonding interactions described above link neighbouring complexes into a 2D hydrogen bonded network (Fig. 5). Packing in $[Fe(\mathbf{L_2})_2](NO_3)\cdot H_2O$ is slightly different in that the nitrate counter anion does not act as a bridge between two thioamide NH groups on neighbouring complex molecules. Instead the nitrate anion acts as an acceptor in a hydrogen bond to one thioamide NH

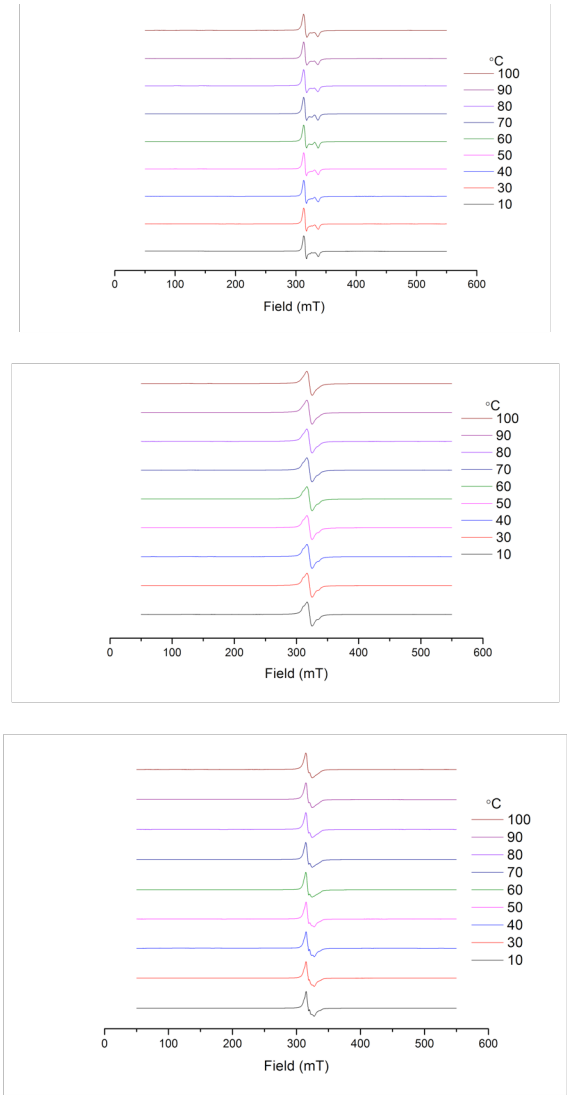

Fig. 6 Variable temperature EPR of $[Fe(\mathbf{L_1})_2](NO_3)\cdot H_2O$ (top), $[Fe(\mathbf{L_2})_2](NO_3)\cdot H_2O$ (middle) and $[Fe(\mathbf{L_3})_2](NO_3)\cdot$ ¾H_2O (bottom).

[N(21)···O(100) = 2.822(4) Å and <(N(21)-H(21)···O(100))= 171°] and also to the interstitial water [O(200)···O(100)' = 2.797(5) Å and <(O(200)-H(20A) ···O(100)')= 172°]. This in turn acts as the acceptor to the other thioamide NH [N(1)···O(200)' = 2.885(5) Å and <(N(1)-H(1)···O(200))= 174°]. The end result is the linking of molecules through H-bonding interactions to the nitrate and interstitial water molecules giving rise to a complex H-bonding network (Fig. 5). Packing in $[Fe(\mathbf{L_3})_2](NO_3)\cdot$¾$H_2O$ is similar to that of $[Fe(\mathbf{L_2})_2](NO_3)\cdot H_2O$. Again, the nitrate anion acts as an acceptor in a hydrogen bond to one thioamide NH [N(1)···O(102)' = 2.929(15) Å and <(N(1)-H(1)···O(102)')= 151°] and also to the interstitial water [O(200)···O(102)' = 2.888(16) Å and <(O(200)-H(20B) ···O(102)')= 169°]. This in turn acts as the acceptor to the other thioamide NH [N(21)···O(200) = 3.008(15) Å and <(N(21)-H(21)···O(200))= 172°]. Overall, the packing in these Fe(III) systems is complex and extensive, and there are multiple supramolecular connections that link neighbouring molecules within the crystal structure (Fig. S46, ESI).

3.5 Crystallographic analysis of Co^{3+} complexes

Crystals of $[Co(\mathbf{L_1})_2](BF_4)\cdot H_2O$, $[Co(\mathbf{L_2})_2](BF_4)\cdot Et_2O$, and $[Co(\mathbf{L_3})_2](BF_4)$ were also obtained as red plate-like crystals by

diffusion of diethyl ether into methanolic solutions of the complexes and the Low temperature (100 K) structures studied. $[Co(\mathbf{L_1})_2](BF_4)\cdot H_2O$ crystallised in the monoclinic space group $P2_1/n$, $[Co(\mathbf{L_2})_2](BF_4)\cdot Et_2O$ in the monoclinic space group $P2_1/c$ and $[Co(\mathbf{L_3})_2](BF_4)$ in the orthorhombic space group *Pbca*. The general structure of each complex is similar to the Fe(III) systems where the Co(III) centre adopts a distorted octahedral geometry with a S_2N_4 coordination sphere. In the Co(III) systems the coordination geometries are closer to pure octahedral than the Fe(III) analogues (distortion parameter Σ range = 48.5 – 53.6°). Packing interactions are also somewhat similar to the Fe(III) versions with the exception of $[Co(\mathbf{L_2})_2](BF_4)\cdot Et_2O$ which has a disordered partial occupancy Et_2O molecule within the crystal lattice. $[Co(\mathbf{L_1})_2](NO_3)\cdot H_2O$ displays hydrogen bonding interactions between the thioamide NH groups on neighbouring complexes (N(4)' and N(24)) and a tetrafluoroborate counter anion [N(4)'···F(4) = 2.896(3) Å and <(N(4)'-H(4X)'···F(4))= 171°; N(24)···F(4) = 2.882(4) Å and <(N(24)-H(24X)···F(4))= 161°] where the BF_4^- acts as a bridge between two complex molecules

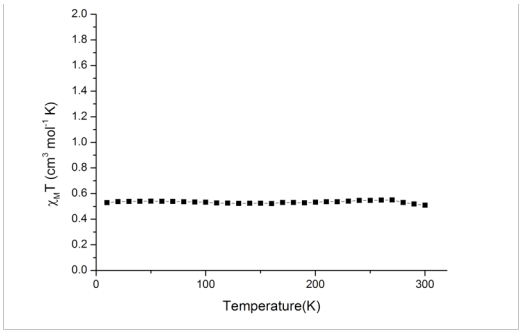

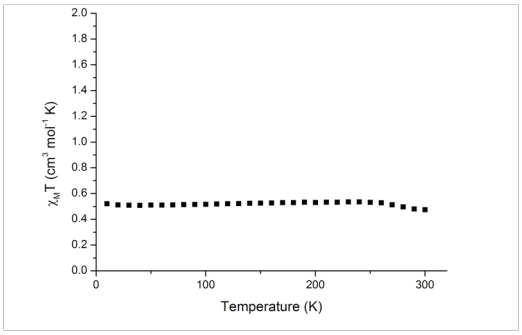

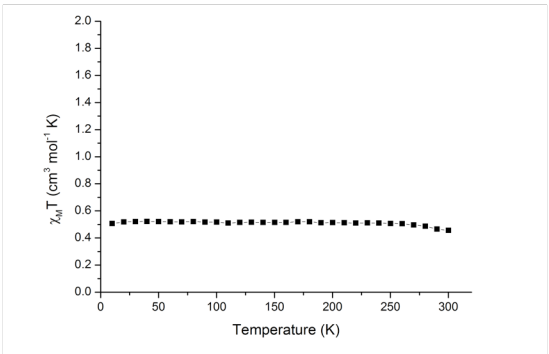

Fig 7 Plots of χ_MT vs. T for $[Fe(\mathbf{L_1})_2](NO_3)\cdot H_2O$ (top), $[Fe(\mathbf{L_2})_2](NO_3)\cdot H_2O$ (middle) and $[Fe(\mathbf{L_3})_2](NO_3)\cdot$ ¾H_2O (bottom).

(Fig S41, ESI). The interstitial water molecule further bridges the tetrafluoroborate anion to a third complex molecule by acting as a hydrogen bond donor to two tetrafluoroborate fluorine atoms (F(1) & F(2)) and the thioenolate nitrogen atom (N(23)') on a neighbouring molecule [O(1)···F(1) = 3.001(5) Å and <(O(1)-H(10Y) ···F(1))= 160°;[O(1)···F(2) = 3.169(6) Å and <(O(1)-H(10Y) ···F(2))= 138°; O(1)···N(23)" = 2.861(5) Å and <(O(1)-H(10X)···N(23)")= 165°]. The NH and OH hydrogen bonding interactions described above link neighbouring complexes into a 2D hydrogen bonded network. Packing in $[Co(\mathbf{L_2})_2](BF_4)\cdot H_2O$ is slightly different in that the tetrafluoroborate counter anion does not act as a bridge between two thioamide NH groups on neighbouring complex molecules. Instead neighbouring complexes interact directly with each other through the thioamide NH and an adjacent thioamide S [N(24)···S(2)' = 3.428(3) Å and <(N(24)-H(24X)···S(2)')= 159°] and the thioamide NH with the tetrafluoroborate counter anion [N(4)···F(1) = 2.883(4) Å and <(N(4)-H(4) ···F(1))= 145°].

3.6 Electron Paramagnetic Resonance and Magnetism

Variable temperature X-band EPR also confirmed the predominantly low spin nature of these complexes. Measurements on all complexes, between 283 and 373 K, exhibit a g factor of *ca.* 2.1, indicative of low spin Fe(III) complexes (Fig. 6). Variable temperature magnetic susceptibility measurements were obtained for crystalline samples of $[Fe(\mathbf{L_1})_2](NO_3)\cdot H_2O$, $[Fe(\mathbf{L_2})_2](NO_3)\cdot H_2O$, and $[Fe(\mathbf{L_3})_2](NO_3)\cdot ¾H_2O$ between 10 and 400 K in an applied field of 1000 *Oe*. All three Fe(III) complexes exhibit very similar properties with a static χ_MT value of 0.5 cm^3 mol^{-1} K between 10 and 300 K (Fig. 7). The S = 1/2 low spin assignment at low temperatures is in accordance with the bond lengths of approximately 2 Å for the Fe-N donors.

4. Conclusions

We have reported on the synthesis and characterisation of six new Fe(III) and Co(III) complexes prepared from novel thiosemicarbazone ligands. Variable temperature magnetic measurements and EPR spectra of the Fe(III) systems showed that they adopted a low spin configuration from 10 – 300 K. The complexes displayed significant solution stability, as assessed through electronic spectra for Fe(III) complexes and NMR spectra for Co(III) complexes run four weeks apart. The solid-state structures displayed many intermolecular interactions linking the complexes into intricate arrays. The combination of significant structure extension through supramolecular interactions and solution stability is ideal for the development of supramolecular materials as the systems should be suitable for a variety of immobilisation techniques where solution processability is required (*e.g.* gels, Langmuir-Blodgett films and incorporation into polymers). We are currently investigating the development of such systems through incorporation of structure directing substituents into the ligands. Additionally, the ligand family presented herein is similar to known SCO ligands, thus it represents an upper limit to ligand field strength, laying the foundation for tailored design of these ligands for highly processable solution-stable SCO species. Addition of electron-withdrawing groups to the thiazole ring is expected to favourably alter the ligand field strength.

Acknowledgements

The authors are grateful to the University of Southampton and University College Dublin for support of this work. JAK thanks the EPSRC for funding through grant references

EP/K039466/1 and EP/K014382/1. ABC thanks the Leverhulme Trust for the award of a Study Abroad Studentship (SAS2016-38). GGM would like to thank Science Foundation Ireland for Investigator Project Award 12/IP/1703, The National University of Ireland and the Cultural Service of the French Embassy in Ireland for scholarships (to A.J.F) and the Irish Higher Education Authority for funding for a SQUID magnetometer.

References

1 J. P. Byrne, J. A. Kitchen and T. Gunnlaugsson, Chem. Soc. Rev. Chem., 2014, 43, 5302–5325.
2 J. E. M. Lewis, E. L. Gavey, S. A. Cameron and J. D. Crowley, Chem. Sci., 2012, 3, 778–784.
3 D. J. Wales and J. A. Kitchen, Chem. Cent. J., 2016, 10, 72.
4 A. Ferguson, R. W. Staniland, C. M. Fitchett, M. A. Squire, B. E. Williamson and P. E. Kruger, Dalton Trans., 2014, 43, 14550–14553.
5 S. Shanmugaraja, C. Dabadie, K. Byrne, A. J. Savyasachi, D. Umadevi, W. Schmitt, J. A. Kitchen and T. Gunnlaugsson, Chem. Sci., 2017, 8, 1535-1546.
6 C. Bartual-Murgui, A. Akou, C. Thibault, G. Molnár, C. Vieu, L. Salmon and A. Bousseksou, J. Mater. Chem. C, 2015, 3, 1277–1285.
7 S. Ji, W. Wu, W. Wu, P. Song, K. Han, Z. Wang, S. Liu, H. Guo and J. Zhao, J. Mater. Chem., 2010, 20, 1953–1963.
8 V. W-W. Yam and K. M-C. Wong, Chem. Commun., 2011, 47, 11579–11592.
9 M. Galli, J. E. M. Lewis and S. M. Goldup, Angew. Chem. Int. Ed., 2015, 54, 13545–13549.
10 D. J. Harding, W. Phonsri, P. Harding, I. A. Gass, K. S. Murray, B. Moubaraki, J. D. Cashion, L. Liu and S. G. Telfer, Chem. Commun., 2013, 49, 6340–6342.
11 M. J. Murphy, T. D. Keene, J. R. Price, D. M. D'Alessandro and C. J. Kepert, Aust. J. Chem., 2014, 67, 1607–1611.
12 R. E. Powell, C. H. Schwalbe, G. J. Tizzard and P. J. van Koningsbruggen, Acta Crystallogr. Sect. C Struct. Chem., 2014, 70, 595–598.
13 S. Floquet, E. Rivière, K. Boukheddaden, D. Morineau and M.-L. Boillot, Polyhedron, 2014, 80, 60–68.
14 Z.-Y. Li, J.-W. Dai, Y. Shiota, K. Yoshizawa, S. Kanegawa and O. Sato, Chem. Eur. J., 2013, 19, 12948–12952.
15 Z.-Y. Li, J.-W. Dai, K. J. Gagnon, H.-L. Cai, T. Yamamoto, Y. Einaga, H.-H. Zhao, S. Kanegawa, O. Sato, K. R. Dunbar and R.-G. Xiong, Dalton Trans., 2013, 42, 14685–14688.
16 E. W. Y. Tido, C. Faulmann, R. Roswanda, A. Meetsma and P. J. van Koningsbruggen, Dalton Trans., 2010, 39, 1643–1651.
17 S. Floquet, M. C. Muñoz, R. Guillot, E. Rivière, G. Blain, J.-A. Réal and M.-L. Boillot, Inorg. Chim. Acta, 2009, 362, 56–64.
18 J. A. Kitchen, N. G. White, G. N. L. Jameson, J. L. Tallon and S. Brooker, Inorg. Chem., 2011, 50, 4586–4597.
19 J. A. Kitchen, A. Noble, C. D. Brandt, B. Moubaraki, K. S. Murray and S. Brooker, Inorg. Chem., 2008, 47, 9450–9458.
20 J. A. Kitchen, N. G. White, M. Boyd, B. Moubaraki, K. S. Murray, P. D. W. Boyd and S. Brooker, Inorg. Chem., 2009, 48, 6670–6679.
21 J. A. Kitchen, J. Olguín, R. Kulmaczewski, N. G. White, V. A. Milway, G. N. L. Jameson, J. L. Tallon and S. Brooker, Inorg. Chem., 2013, 52, 11185–11199.
22 J. A. Kitchen, G. N. L. Jameson, J. L. Tallon and S. Brooker, Chem. Commun., 2010, 46, 3200–3202.
23 N. G. White, H. L. C. Feltham, C. Gandolfi, M. Albrecht and S. Brooker, Dalton Trans., 2010, 39, 3751–3758.
24 M. Cavallini, Phys. Chem. Chem. Phys., 2012, 14, 11867–11876.
25 J. A. Kitchen, N. Zhang, A. B. Carter, A. J. Fitzpatrick and G. G. Morgan, J. Coord. Chem., 2016, 69, 2024–2037.
26 A. J. Fitzpatrick, P. N. Martinho, B. J. Gildea, J. D. Holbrey and G. G. Morgan, Eur. J. Inorg. Chem., 2016, 2025–2029.
27 P. N. Martinho, C. J. Harding, H. Müller-Bunz, M. Albrecht and G. G. Morgan, Eur. J. Inorg. Chem., 2010, 675–679.
28 E. N. W. Howe, N. Busschaert, X. Wu, S. N. Berry, J. Ho, M. E. Light, D. D. Czech, H. A. Klein, J. A. Kitchen and P. A. Gale, J. Am. Chem. Soc., 2016, 138, 8301–8308.
29 B. Ghosh, P. Adak, S. Naskar, B. Pakhira, P. Mitra, R. Dinda, S. K. Chattopadhyay, Inorg. Chim. Acta., 2017, 459, 1–14.
30 N. A. Ryabova, V. I. Ponomarev, V. V. Zelentsov, V. I. Shipilov and L. O. Atovmyan, J. Struct. Chem., 1981, 22, 234–238.
31 J. R. Dilworth and R. Hueting, Inorg. Chim. Acta., 2012, 389, 3–15.
32 N. C. Saha, A. Saha, R. J. Butcher, S. Chaudhuri and N. Saha, Inorg. Chim. Acta, 2002, 339, 348–354.
33 M. M. M. Raposo, B. García-Acosta, T. Ábalos, P. Calero, R. Martínez-Máñez, J. V. Ros-Lis and J. Soto, J. Org. Chem., 2010, 75, 2922–2933.
34 R. Venkatraman, H. Ameera, L. Sitole, E. Ellis, F. R. Fronczek and E. J. Valente, J. Chem. Crystallogr., 2009, 39, 711–718.
35 R. Venkatraman, M. A. Hossain and F. R. Fronczek, Acta Crystallogr. Sect. E Struct. Rep. Online, 2010, 66, 541–542.
36 R. Venkatraman, D. S. Samuel, Z. Arslan, M. A. Hossain and F. R. Fronczek, Acta Crystallogr. Sect. E Struct. Rep. Online, 2013, 69, 246–247.
37 S. R. Arumugam, S. S. R. Dasary, R. Venkatraman, H. Yu and F. R. Fronczek, Acta Crystallogr. Sect. E Struct. Rep. Online, 2011, 67, 1409–1410.
38 S. S. R. Dasary, S. R. Arumugam, H. Yu, R. Venkatraman and F. R. Fronczek, Acta Crystallogr. Sect. E Struct. Rep. Online, 2011, 67, 816–817.
39 S. J. Coles and P. A. Gale, Chem. Sci., 2012, 3, 683–689.
40 CrystalClear-SM Expert 3.1, (Rigaku, 2012).
41 CrysAlisPro 38.41, (Rigaku Oxford Diffraction, 2015).
42 G. M. Sheldrick, Acta Crystallogr. A, 2008, 64, 112–122.
43 O. V. Dolomanov, L. J. Bourhis, R. J. Gildea, J. A. K. Howard and H. Puschmann, J. Appl. Crystallogr., 2009, 42, 339–341.
44 R. G. Miller and S. Brooker, Inorg. Chem., 2015, 54, 5398–5409.
45 J. Nelson, V. McKee, G. Morgan, Prog. Inorg. Chem. 1998, 47, 167–317

.